Smart Structures and Systems, Vol. 5, No. 3 (2009) 291-316
DOI: http://dx.doi.org/10.12989/sss.2009.5.3.291

Damage detection for truss or frame structures using an axial strain flexibility

Guirong Yan*, Zhongdong Duan‡ and Jinping Ou‡†

School of Civil Engineering, Harbin Institute of Technology, Harbin, 150090, China

(Received April 2, 2008, Accepted November 25, 2008)

Abstract. Damage detection using structural classical deflection flexibility has received considerable attention due to the unique features of the flexibility in the last two decades. However, for relatively complex structures, most methods based on classical deflection flexibility fail to locate damage sites to the exact members. In this study, for structures whose members are dominated by axial forces, such as truss structures, a more feasible flexibility for damage detection is proposed, which is called the Axial Strain (AS) flexibility. It is synthesized from measured modal frequencies and axial strain mode shapes which are expressed in terms of translational mode shapes. A damage indicator based on AS flexibility is proposed. In addition, how to integrate the AS flexibility into the Damage Location Vector (DLV) approach (Bernal and Gunes 2004) to improve its performance of damage localization is presented. The methods based on AS flexbility localize multiple damages to the exact members and they are suitable for the cases where the baseline data of the intact structure is not available. The proposed methods are demonstrated by numerical simulations of a 14-bay planar truss and a five-story steel frame and experiments on a five-story steel frame.

Keywords: axial strain; flexibility; damage detection; damage localization.

1. Introduction

Techniques for damage detection based on structural classical deflection flexibility have received considerable attention due to the following unique features of the flexibility matrix. One is that the flexibility matrix can be estimated from a truncated set of lower frequency modes with sufficient accuracy. And the other is that flexibility matrix at the measurement sensor coordinates can be extracted from the matrices of system realization. Researches on how to construct the complete structural flexibility from the measured modes have been conducted by some researchers (Doebling, *et al*. 1996, Doebling and Peterson 1997, Doebling and Farrar 1996).

Using numerical examples of different types of beams and experiments on a free-free beam, Pandey and Biswas (1994, 1995) demonstrated that the change in structural flexibility from the pre-damaged to post-damaged states could be used to locate the damage occurred in beam type structures. However, this method has some disadvantages as follows. First, the change in structural flexibility is affected by different support conditions of the structures, and thus the information on the types of the structures should be available in advance; second, for some structures with free boundary condition at one end,

*E-mail: yan.g@seas.wustl.edu
‡Corresponding Author, E-mail: duanzd@hit.edu.cn
‡†E-mail: oujinping@hit.edu.cn

this method fails to locate multiple damage sites.

Since the damage detection results using classical deflection flexibility mentioned above are manifested as nodes or DOFs (Degrees Of Freedom) characterization, these methods are difficult to localize damages in structures which have load-path redundancy. Consequently, it seems reasonable to detect damage using the localized flexibility based methods which project damages on substructures or elements (Reich and Park 2000, Park, *et al.* 1997). Central to this kind of methods is to decompose the global flexibility into localized substructural flexibility or elemental flexibility. Doebling and Peterson (1998) extracted substructural flexibility from the measured flexibility based on the projection of the experimentally measured flexibility onto the strain energy distribution in local elements or regional superelements, while Park and Felippa (1998) accomplished it through a complete variational decomposition of the energy functional of the dynamic system.

Apart from the localized flexibility based methods, the Damage Locating Vector (DLV) approach developed by Bernal and Gunes (2004) also has the ability to map change in measured deflection flexibility to responsible elements in the structure. The basic idea is that when the Damage Locating Vectors (DLVs) that span the null-space of the flexibility change are treated as static loads and applied on the intact structure, they lead to stress fields whose magnitudes are zero in the damaged elements. Gao and Spencer (2002) extended the the DLV approach to the case of ambient vibration using a modal expansion technique, while Bernal and Gunes (2002) and Duan, *et al*. (2005) realized this through using a proportional flexibility matrix constructed by different algorithms, respectively.

To directly project damages onto elements or superelements instead of nodes or DOFs when only a few lower frequency translational modes are available, Duan, *et al*. (2005) defined a more feasible flexibility for damage detection of beam type structures, which was called the Angle-between-String-and-Horizon (ASH) flexibility. Physically, the elements in the *i*th column of ASH flexibility represent the Angles-between-String-and-Horizon (ASHs) of each element resulting from a unit moment in the form of a pair of parallel forces with equal amplitudes but opposite directions applied at the two nodes of the *i*th element. The diagonal entries or the maximum absolute values of the elements in each column of the difference between the ASH flexibilities for the pre- and post-damaged structures were designated as the damage indicators of the corresponding elements. Multiple damage locations can be directly indicated by step distribution of the proposed damage indicators and it was true for structures with arbitrary support conditions. Moreover, this method can determine qualitatively the severity of each damage from the magnitudes of steps. The effectiveness of the method has been demonstrated through numerical simulations and experiments of a cantilever beam and a simply supported beam.

To extend the idea of ASH flexibility to structures whose main internal forces are axial forces, such as truss structures and some frame structures under some specific loads, this study will propose another generalized flexibility for damage detection of this kind of structures, which is the Axial Strain (AS) flexibility. And then three damage detection methods based on the AS flexibility are developed. The basic idea of these methods is that if the members in a structure are dominated by axial forces, the axial strain will be a better index than deflection for damage detection.

The remainder of this paper is organized as follows. First, the AS flexibility is defined and the expression of AS flexibility in terms of the translational modes is derived. Second, two damage detection techniques which are the difference method and the Damage Locating Vector (DLV) method are applied to the AS flexibility matrix, and the direct method using the damaged AS flexibility is proposed for cases where the baseline data of the intact structure is not available. Third, the performance of the damage detection methods based on AS flexibility is validated by numerical simulations of a planar truss and a steel frame and experiments on a steel frame. Finally, the paper is concluded.

2. Derivation of the axial strain flexibility

For structures whose members are dominated by axial forces, the Axial Strain (AS) flexibility is proposed in this section. Analogy to the definition of Angle-between-String-and-Horizon Flexibility (ASHF) (Duan, *et al.* 2005), the elements in the *i*th column of the AS Flexibility represent the axial strains of all elements or members resulted from a pair of axial forces with equal amplitudes, which are equal to the reciprocals of the length of the *i*th member, but opposite directions applied at two nodes of the *i*th member. This definition is based on the force-bearing characteristics of this kind of structures.

Let's consider a truss with n elements (or members) shown in Fig. 1 to derive the expression of the AS flexibility in terms of translational modes. In this figure, normal and bold numbers indicate node numbers, and italic and bold numbers indicate element (or member) numbers. The DOF numbers for the *i*th node are $2i$-1 and $2i$. Assume that the length of the *k*th element is l_k and the cosine and sine values of the angles between the *k*th member and the *x*-axis in the global coordinate system are c_k and s_k, respectively. To obtain the element ASF_{ji} in the AS flexibility matrix, a pair of axial compression forces with equal amplitudes of $1/l_i$ and opposite directions is applied at two nodes of the *i*th member, and zero forces at all other members. Without loss of generality, the *i*th and *j*th members are assumed to be diagonal members. Herein, the DOF numbers for the two nodes of the *i*th member are ($2d$-1, $2d$, $2g$-1,$2g$), and the DOF numbers for the two nodes of the *j*th member are ($2o$-1, $2o$, $2p$-1,$2p$).

From the physical significance of the AS flexibility, ASF_{ji} is the axial strain of the *j*th member under the action of this pair of forces $1/l_i$, which is equal to the axial deformation of the *j*th member divided by its length. According to the Superimposition Theory of Loads, under this pair of forces, the displacement at each DOF of the *j*th member is equal to the summation of that resulting from each individual force. When an axial compression force with amplitude of $1/l_i$ is applied at Node *d*, this force is decomposed into horizontal and vertical components with amplitudes c_i/l_i and s_i/l_i, respectively, as shown in Fig. 1. From the physical meaning of the classical deflection flexibility **F**, the displacements at the four DOFs ($2o$-1, $2o$, $2p$-1, $2p$) of the *j*th member resulting from the component force c_i/l_i are $X_{2o\text{-}1}=c_i/l_i\times\mathbf{F}_{2o,2d\text{-}1}$, $X_{2o}=c_i/l_i\times\mathbf{F}_{2o,2d\text{-}1}$, $Y_{2p\text{-}1}=c_i/l_i\times\mathbf{F}_{2p\text{-}1,2d\text{-}1}$ and $X_{2p}=c_i/l_i\times\mathbf{F}_{2p,2d\text{-}1}$, respectively. Likewise, the displacements at these four DOFs resulting from other component forces can also be obtained. And thus the total displacement at each DOF of the *j*th member is the summation of the displacements resulting from the four component forces.

Therefore, the total deformation in the x and y direction of the *j*th member (δX_j and δY_j) induced by this pair of forces at the two nodes **g** and **d** of the *i*th member is expressed as

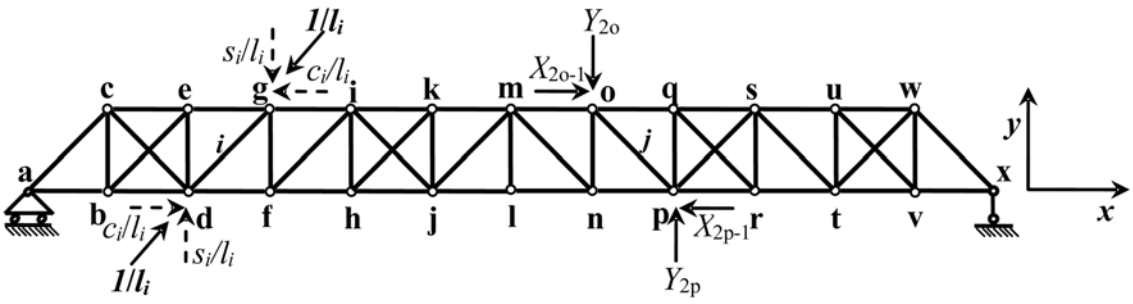

Fig. 1 The definition of the Axial Strain Flexibility

$$\delta X_j = \frac{c_i}{l_i}(\mathbf{F}_{2o\text{-}1,\,2d\text{-}1} - \mathbf{F}_{2o\text{-}1,\,2g\text{-}1} - \mathbf{F}_{2p\text{-}1,\,2d\text{-}1} + \mathbf{F}_{2p\text{-}1,\,2g\text{-}1}) + \frac{s_i}{l_i}(\mathbf{F}_{2o\text{-}1,\,2d} - \mathbf{F}_{2o\text{-}1,\,2g} - \mathbf{F}_{2p\text{-}1,\,2d} + \mathbf{F}_{2p\text{-}1,\,2g}) \tag{1}$$

$$\delta Y_j = \frac{c_i}{l_i}(\mathbf{F}_{2p,\,2d\text{-}1} - \mathbf{F}_{2p,\,2g\text{-}1} - \mathbf{F}_{2o,\,2d\text{-}1} + \mathbf{F}_{2o,\,2g\text{-}1}) + \frac{s_i}{l_i}(\mathbf{F}_{2p,\,2d} - \mathbf{F}_{2p,\,2g} - \mathbf{F}_{2o,\,2d} + \mathbf{F}_{2o,\,2g}) \tag{2}$$

where $\mathbf{F}$ is the classical deflection flexibility which is assembled from the translational modes as

$$\mathbf{F} = \mathbf{\Phi}\mathbf{\Omega}^{-1}\mathbf{\Phi}^{\mathrm{T}} = \sum_{r=1}^{n} \frac{1}{\omega_r^2}\boldsymbol{\varphi}_r\boldsymbol{\varphi}_r^{\mathrm{T}} \tag{3}$$

where ω_r is the rth circular modal frequency; $\mathbf{\Omega}$ is the diagonal eigenvalue matrix with squares of ω_r ($r = 1,\ldots,n$) as its diagonals; $\mathbf{\Phi}$ is the mode shape matrix; $\boldsymbol{\varphi}_r$ is the rth mode shape; n is the number of measured modes. $\mathbf{F}_{ji}$ is one element in $\mathbf{F}$ which represents the displacement at DOF j resulting from a unit force applied at DOF i and is obtained as

$$\mathbf{F}_{ji} = \sum_{r=1}^{n} \frac{1}{\omega_r^2}\varphi_{jr}\varphi_{ir} \tag{4}$$

where φ_{ir} and φ_{jr} are the ith and jth entries of the rth mode shape, respectively.

Then the axial deformation of the jth member is

$$\delta l_j = c_j\delta X_j - s_j\delta Y_j \tag{5}$$

and the axial strain of the jth member is

$$\mathrm{ASF}_{ji} = \frac{\delta l_j}{l_j} = \frac{c_j\delta X_j - s_j\delta Y_j}{l_j} \tag{6}$$

With Eq. (4) in mind, substituting Eq. (1) and Eq. (2) into Eq. (6), we obtain ASF_{ji} as follows

$$\begin{aligned}\mathrm{ASF}_{ji} = \sum_{r=1}^{n}\frac{1}{\omega_r^2}\Bigg(&\frac{c_j}{l_j}\Bigg(\frac{c_i}{l_i}\left(\varphi_{2o-1,r}\varphi_{2d-1,r} - \varphi_{2o-1,r}\varphi_{2g-1,r} - \varphi_{2p-1,r}\varphi_{2d-1,r} + \varphi_{2p-1,r}\varphi_{2g-1,r}\right)\\ &+\frac{s_i}{l_i}\left(\varphi_{2o-1,r}\varphi_{2d,r} - \varphi_{2o-1,r}\varphi_{2g,r} - \varphi_{2p-1,r}\varphi_{2d,r} + \varphi_{2p-1,r}\varphi_{2g,r}\right)\Bigg)\\ &-\frac{s_j}{l_j}\Bigg(\frac{c_i}{l_i}\left(\varphi_{2p,r}\varphi_{2d-1,r} - \varphi_{2p,r}\varphi_{2g-1,r} - \varphi_{2o,r}\varphi_{2d-1,r} + \varphi_{2o,r}\varphi_{2g-1,r}\right)\\ &+\frac{s_i}{l_i}\left(\varphi_{2p,r}\varphi_{2d,r} - \varphi_{2p,r}\varphi_{2g,r} - \varphi_{2o,r}\varphi_{2d,r} + \varphi_{2o,r}\varphi_{2g,r}\right)\Bigg)\Bigg)\end{aligned} \tag{7a}$$

Eq. (7a) are further formulated, and the expression of ASF_{ji} in terms of translational modes is written as

$$\begin{aligned}\mathrm{ASF}_{ji} = \sum_{r=1}^{n} \frac{1}{\omega_r^2} \Bigg(& c_j c_i \frac{(\varphi_{2o-1,r} - \varphi_{2p-1,r})}{l_j} \frac{(\varphi_{2d-1,r} - \varphi_{2g-1,r})}{l_i} + c_j s_i \frac{(\varphi_{2o-1,r} - \varphi_{2p-1,r})}{l_j} \frac{(\varphi_{2d,r} - \varphi_{2g,r})}{l_i} \\ & + s_j c_i \frac{(\varphi_{2o,r} - \varphi_{2p,r})}{l_j} \frac{(\varphi_{2d-1,r} - \varphi_{2g-1,r})}{l_i} + s_j s_i \frac{(\varphi_{2o,r} - \varphi_{2p,r})}{l_j} \frac{(\varphi_{2d,r} - \varphi_{2g,r})}{l_i} \Bigg) \\ = \sum_{r=1}^{n} \frac{1}{\omega_r^2} & \left(c_j \frac{\varphi_{2o-1,r} - \varphi_{2p-1,r}}{l_j} + s_j \frac{\varphi_{2o,r} - \varphi_{2p,r}}{l_j} \right) \left(c_i \frac{\varphi_{2d-1,r} - \varphi_{2g-1,r}}{l_i} + s_i \frac{\varphi_{2d,r} - \varphi_{2g,r}}{l_i} \right)\end{aligned} \tag{7b}$$

Similarly, computing the axial strains of all other elements under this pair of forces, we obtain all other entries in the *i*th column of the AS flexibility. And thus the *i*th column of AS flexibility can be expressed as

$$\mathrm{ASF}_i = \sum_{r=1}^{n} \frac{1}{\omega_r^2} \mathbf{S}_r \left(c_i \frac{(\varphi_{2d-1,r} - \varphi_{2g-1,r})}{l_i} + s_i \frac{(\varphi_{2d,r} - \varphi_{2g,r})}{l_i} \right) \tag{8}$$

in which

$$\mathbf{S}_r = \begin{pmatrix} c_1 \dfrac{(\varphi_{2a-1,r} - \varphi_{2b-1,r})}{l_1} + s_1 \dfrac{(\varphi_{2a,r} - \varphi_{2b,r})}{l_1} \\ \cdots \\ c_j \dfrac{(\varphi_{2o-1,r} - \varphi_{2p-1,r})}{l_j} + s_j \dfrac{(\varphi_{2o,r} - \varphi_{2p,r})}{l_j} \\ \cdots \\ c_n \dfrac{(\varphi_{2w-1,r} - \varphi_{2x-1,r})}{l_n} + s_n \dfrac{(\varphi_{2w,r} - \varphi_{2x,r})}{l_n} \end{pmatrix} \tag{9}$$

where $\mathbf{S}_r$ is called the *r*th axial strain mode shape and its *j*th component $c_j \frac{(\varphi_{2o\text{-}1,r} - \varphi_{2p\text{-}1,r})}{l_j} + s_j \frac{(\varphi_{2o,r} - \varphi_{2p,r})}{l_j}$ is associated with the *j*th member instead of a DOF or a node.

Likewise, to apply a pair of axial forces with equal amplitudes but opposite directions at two nodes of another member and compute the axial strains of all elements, another column of the AS flexibility matrix is to be obtained.

Stacking all columns in a matrix, we can assemble the AS flexibility matrix as

$$\mathrm{ASF} = \sum_{r=1}^{n} \frac{1}{\omega_r^2} \mathbf{S}_r \mathbf{S}_r^T \tag{10}$$

Comparing Eq. (10) with Eq. (3), one can observe the similarity between the AS flexibility and classical deflection flexibility except that the axial strain mode shapes are utilized in Eq. (10) instead of the translational mode shapes. However, each element in the AS flexibility is associated with a structural member or element, while each element in classical deflection flexibility is associated with a

structural DOF.

If the ith element is horizontal and the jth element is vertical, c_i=1, s_i=0, c_j=0 and s_j=1. Then Eq. (7b) can be simplified as

$$\begin{aligned} \mathrm{ASF}_{ji} &= -\frac{1}{l_j}\left(\frac{1}{l_i}\left(\mathbf{F}_{2p,2d-1}-\mathbf{F}_{2p,2g-1}\right)-\frac{1}{l_i}\left(\mathbf{F}_{2o,2d-1}-\mathbf{F}_{2o,2g-1}\right)\right) \\ &= \sum_{r=1}^{n}\frac{1}{\omega_r^2}\frac{\left(\varphi_{2o,r}-\varphi_{2p,r}\right)}{l_j}\frac{\left(\varphi_{2d-1,r}-\varphi_{2g-1,r}\right)}{l_i} \end{aligned} \tag{11}$$

For a statically determined structure under loads, if a given local part of the structure can balance the loads applied on this part, only the members in this part bear forces, while the other members are free to loads (Long and Bao 1996), which is the basic idea of the Local Balancing Theory. According to this theory, for a statically determined truss, when a pair of axial forces with equal magnitudes and opposite directions is applied at two nodes of a member, only this member bears force and produces axial deformation, whereas the axial deformations in all other members are necessarily zero. Therefore, the AS flexibility matrix is theoretically diagonal for a statically determined truss. However, because only a few low frequency modes are identified in practical engineerings, the AS flexibility matrix constructed from the incomplete set of modes is not ideally diagonal.

For a space truss with n elements, the rth axial strain mode shape $\mathbf{S}_r$ can be written as

$$\mathbf{S}_r = \begin{pmatrix} c_1\dfrac{(\varphi_{3a-2,r}-\varphi_{3b-2,r})}{l_1}+s_1\dfrac{(\varphi_{3a-1,r}-\varphi_{3b-1,r})}{l_1}+z_1\dfrac{(\varphi_{3a,r}-\varphi_{3b,r})}{l_1} \\ \cdots \\ c_j\dfrac{(\varphi_{3o-2,r}-\varphi_{3p-2,r})}{l_j}+s_j\dfrac{(\varphi_{3o-1,r}-\varphi_{3p-1,r})}{l_j}+z_j\dfrac{(\varphi_{3o,r}-\varphi_{3p,r})}{l_j} \\ \cdots \\ c_n\dfrac{(\varphi_{3w-2,r}-\varphi_{3x-2,r})}{l_n}+s_n\dfrac{(\varphi_{3w-1,r}-\varphi_{3x-1,r})}{l_n}+z_n\dfrac{(\varphi_{3w,r}-\varphi_{3x,r})}{l_n} \end{pmatrix} \tag{12}$$

where c_i, s_i and z_i are cosine values of the angles between the jth member and the x-axis, y-axis and z-axis in the global coordinate system. Substituting Eq. (12) into Eq. (10), the AS flexibility of the space truss can be obtained.

For a frame structure, if the loads are applied on nodes and the main internal force in each member is dominated by axial force, the axial strain mode shape also can be obtained by Eq. (9) or Eq. (12) and then the AS flexibility matrix of a frame structure can be assembled using Eq. (10).

A more general definition of strain flexibility for any types of structures is referred to Sim and Spencer (2007).

3. Damage detection by the AS flexibility

For the structures whose members are dominated by axial forces, it is obvious that the axial strain can be a better index than deflection for damage detection. Therefore, the proposed AS flexibility is likely to be more suitable for damage detection of this kind of structures than the classical deflection flexibility. In this section, three damage detection methods based on the AS flexibility are developed.

3.1. The AS flexibility difference method

For the member in the state of the axial deformation, the axial strain can be expressed as

$$\varepsilon = \frac{\Delta l}{l} = \frac{N}{EA} \tag{13}$$

where l is the length of the member; E is the Young's modulus and A is the cross-sectional area.

Eq. (13) suggests that the axial strain is inversely proportional to both E and A. Therefore, once the member in the structure is damaged, for example, E or A is reduced, the axial strain increases and so does the associated diagonals of AS flexibility with the member. And thus the change in AS flexibilities from the pre- to post-damaged states can be used to identify damage.

The AS flexibilities for the intact and damaged structures, denoted as ASF^u and ASF^d, respectively, are first constructed by Eq. (10). Then the change in AS flexibility is computed as

$$\Delta\mathrm{ASF} = \mathrm{ASF}^d - \mathrm{ASF}^u \tag{14}$$

The percentage of change in the diagonal element of AS flexibility is designated as the damage indicator of each element

$$\begin{aligned} \delta\mathrm{ASF}d &= [\delta\mathrm{ASF}d_1 \quad \delta\mathrm{ASF}d_2 \ldots \delta\mathrm{ASF}d_i \ldots \delta\mathrm{ASF}d_{n-1} \quad \delta\mathrm{ASF}d_n] \\ &= \left(\frac{\Delta\mathrm{ASF}_{11}}{\mathrm{ASF}^d_{11}} \frac{\Delta\mathrm{ASF}_{22}}{\mathrm{ASF}^d_{22}} \cdots \frac{\Delta\mathrm{ASF}_{ii}}{\mathrm{ASF}^d_{ii}} \cdots \frac{\Delta\mathrm{ASF}_{n\text{-}1,\,n\text{-}1}}{\mathrm{ASF}^d_{n\text{-}1,\,n\text{-}1}} \frac{\Delta\mathrm{ASF}_{n,n}}{\mathrm{ASF}^d_{n,n}}\right) \end{aligned} \tag{15}$$

where i and n denote the element number.

The proposed $\delta\mathrm{ASF}d$ indicators are directly associated with the elements or members in the structure. And the elements associated with the entries in $\delta\mathrm{ASF}d$ with large magnitudes are identified as damaged elements or members. When a complete set of modes are used to assemble the AS flexibility, the fractions in $\delta\mathrm{ASF}d$ represent damage severities with a unit indicating a totally damaged member and zero indicating an undamaged member. In practical applications, if more modes are identified, this indicator is able to qualitatively determine the relative damage extent.

3.2. Damage locating vector approach based on the AS flexibility

The Damage Locating Vectors (DLV) method, developed by Bernal, is an approach for damage localization using change in measured deflection flexibility for the pre- and post-damage states. The fundamental idea of the DLV approach is that when the damage locating vectors (DLVs) that span the null-space of change in flexibility are applied on the undamaged structure as static loads, they induce no stress in the damaged elements (or small stress in the presence of mode truncations or measurement noises). For more details on the DLV method, one can refer to reference (Bernal and Gunes 2004).

In this section, the AS flexibility instead of the classical deflection flexibility is employed to implement the DLV method. To obtain the DLVs, a Singular Value Decomposition (SVD) is first performed on $\Delta\mathrm{ASF}$ as

$$\Delta ASF = USV^T = [U_1\ U_0]\begin{bmatrix} s_1 & 0 \\ 0 & 0 \end{bmatrix}\begin{bmatrix} V_1^T \\ V_0^T \end{bmatrix} \tag{16}$$

For ideal conditions, the DLVs are just V_0 which is the part of the right singular matrix V associated with the null space.

And then the DLVs are applied on two nodes of each member of the intact structure in the form of a pair of axial forces with equal magnitudes and opposite directions. The way of applying forces is detemined by the physical meaning of the proposed AS flexibility, which is quite different from the DLV approach based on classical deflection flexibility.

Next, to calculate the generalized internal force in each member under the loads.

According to the theory of DLV approach, the generalized internal forces (GIFs) in damaged members should be zero or close to zero. Therefore, the damage locations are identified by the GIFs having small magnitudes.

For a statically determined structure, according to the Local Balancing Theory and the Superimposition Theory of Loads, when one set of DLV is applied on the structure as static loads, the component of the DLV is solely borne by the associated member on which it is applied and the internal force (axial force) in this member is just equal to the applied force. And thus the internal force in each member is equal to the corresponding component in the DLV. When all DLVs are applied on the structure, we propose to calculate the total generalized internal force in the *j*th member by one of the following three equations,

$$GIF(j) = \sum_{i=1}^{m} V_0(j, i) \tag{17}$$

$$GIF(j) = \sum_{i=1}^{m} |V_0(j, i)| \tag{18}$$

$$GIF(j) = \sum_{i=1}^{m} (V_0(j, i))^2 \tag{19}$$

where GIF denotes the Generalized Internal Force; *m* indicates the number of the DLVs, which is equal to the column number of V_0.

It is very evident that the procedures for computing the generalized internal force in the DLV approach based on the AS flexibility are much easier than those in the DLV approach based on classical deflection flexibility.

It's interesting to note that if the full set of modes are used in assembling the AS flexibility, the GIFs obtained by the Eq. (19) associated with undamaged elements are unit due to the orthogonality of $\mathbf{V}_0$ and the GIFs of the damaged elements are zero. As to be seen from the following numerical simulation results, the GIF defined by Eq. (19) is better than those by Eq. (17) and Eq. (18) for damage detection.

3.3. The direct method using the damaged AS flexibility

For a structure whose internal forces are dominated by axial forces, such as a frame structure under nodal loads, to obtain the elements in the *i*th column of the AS flexibility matrix, a pair of axial forces

with equal amplitudes but opposite directions is applied at two nodes of the *i*th member and then the axial strains of all members are computed.

On the one hand, when this pair of forces is applied on the *i*th member, only the *i*th member bears large internal force and the axial forces in other members are close to zero because of the rigid connection between members. And thus, we can deduce the AS flexibility matrix of the frame structure is approximately diagonal. On the other hand, because the applied forces on each kind of members (with equal stiffness and equal lengths) are equal, if certain members are damaged, such as the reduction of elastic modulus or cross-sectional area, the axial strain in these members must increase sharply. And accordingly, the diagonal elements in the AS flexibility matrix corresponding with these members also increase. Therefore, for frame structures, the potential damage sites are identified by the maxima of the diagonal elements in the AS flexibility matrix of the damaged structure. Moreover, only few low frequency modes are required.

In addition, for both truss structures and frame structures, if the baseline data of the intact structure can not be readily obtained, damage locations are identified by this method.

4. Numerical examples

4.1. Example #1: A planar truss

By numerical simulations of a planar truss, the performances of the AS flexibility difference method and the DLV based on AS flexibility were investigated.

4.1.1. The analytical model

A 14-bay planar truss structure with simply supports, as shown in Fig. 2, was considered in this example. The cross-sectional area of each member was $1.122\times10^{-4}m^2$. The Young's modulus, mass density and Poisson ratio of the material were 2×10^{11}Pa, 7850 kg/m^3 and 0.3, respectively. The structure had 28 nodes and 53 members. The numbering of elements and nodes of its FEM is shown in Fig. 2. Additional lumped masses of 0.5 kg were applied on the 1st and 28th nodes, and 10 kg on all other nodes.

Damages were simulated as reductions in cross-sectional areas by 10% of the following members: members 3 (a vertical member), 17 (an upper chord member), 27 and 36 (lower chord members), 43, 46 and 51 (diagonal members).

Through the modal analysis in Finite Element Analysis, the first 10 natural frequencies and mode shapes of the intact structure were obtained. The natural frequencies are shown in the column of "Analytical Frequency" in Table 1 and the mode shapes are shown in Fig. 3.

4.1.2. The damage detection results by the as flexibility difference method

4.1.2.1. Results from analytical data

The analytical data was used to illustrate the ASF matrix and the damage indicator based on AS

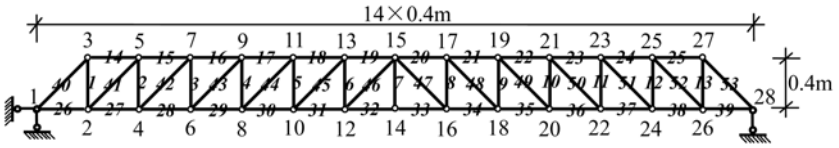

Fig. 2 A 14-bay planar truss

Table 1 Analytical and identified modal parameters of intact and damaged structures

	Intact Case				Damaged Case			
	Analytical Frequency (Hz)	Identified Results			Analytical Frequency (Hz)	Identified Results		
		Frequency (Hz)	Damping ratio (%)	EMAC (%)		Frequency (Hz)	Damping ratio (%)	EMAC (%)
1	8.57	8.57	1.0163	99.82	8.52	8.52	1.0113	99.95
2	29.00	29.00	0.9990	99.88	28.76	28.75	0.9994	99.95
3	42.74	42.73	1.0004	99.93	42.23	42.23	1.0001	99.96
4	57.92	57.91	1.0042	99.55	57.71	57.70	1.0042	99.56
5	88.87	88.84	1.0022	90.82	88.08	88.05	1.0043	92.75
6	117.57	117.51	1.0021	99.52	116.30	116.24	1.0013	99.50
7	122.52	122.45	0.9995	99.80	122.03	121.97	0.9998	99.81
8	148.17	148.06	0.9977	97.67	146.88	146.77	0.9984	99.13
9	171.45	171.28	0.9975	98.01	170.21	170.04	0.9979	98.67
10	190.35	190.11	0.9983	99.55	189.35	189.11	0.9981	99.86

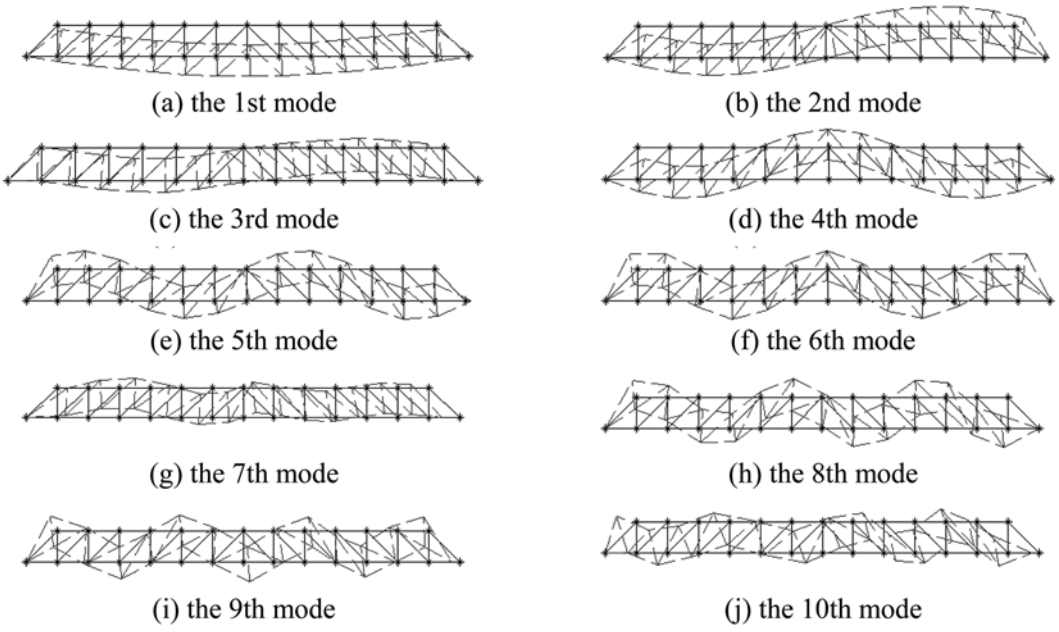

Fig. 3 The first 10 mode shapes of the intact structure

flexibility. Herein, the modal parameters were obtained by Finite Element Analysis.

For the undamaged case, Figs. 4(a) and 4(b) present the AS flexibility matrix and the classical deflection flexibility matrix synthesized from the full set of modes, respectively. It can be seen that the AS flexibility matrix is diagonal when the complete set of modes are used.

The damage indicators based on AS flexibility (δASFd) are plotted against elements in Fig. 5(a). The δASFd indicators associated with the 3rd, 17th, 27th, 36th, 43th, 46th and 51th elements are much larger than those associated with all other elements and are equal to 0.1 which are the relative damage extents of each damaged element. That means that the presented damage indicators not only localize

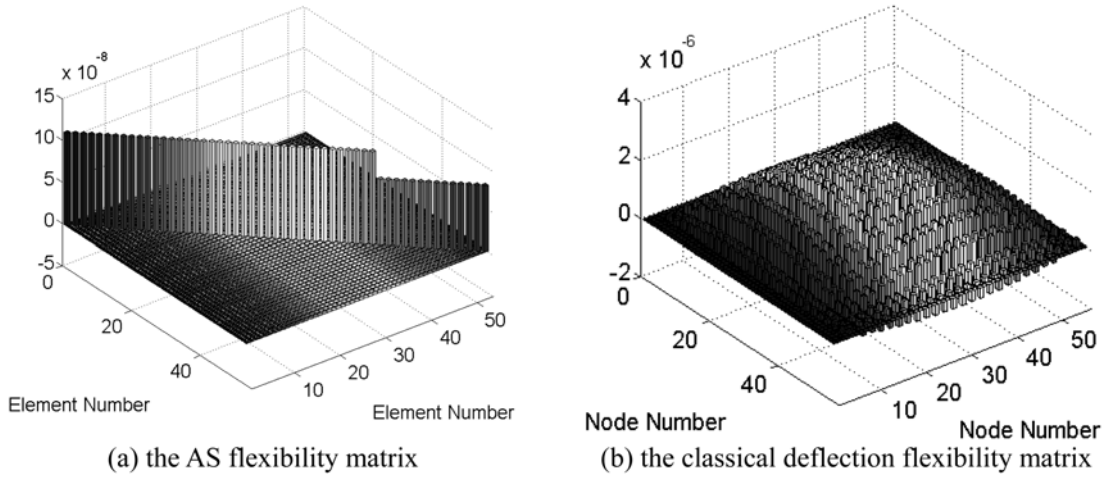

(a) the AS flexibility matrix (b) the classical deflection flexibility matrix

Fig. 4 Flexibility matrices assembled from the complete set of data

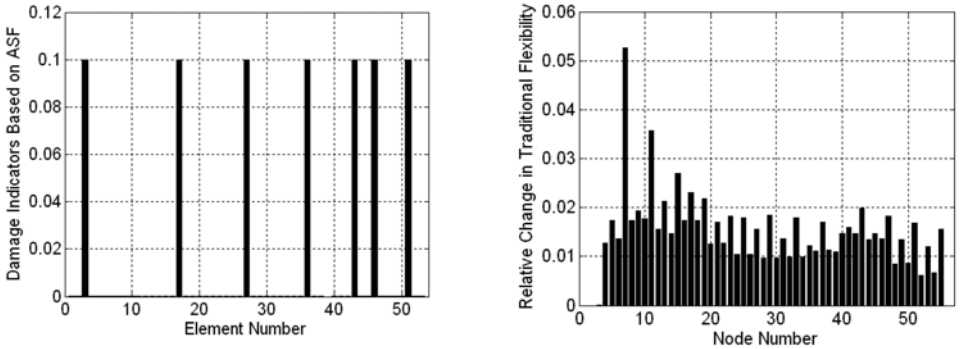

(a) the damage indicators based on AS flexibility (b) the classical deflection flexibility difference method

Fig. 5 Damage detection results using the complete set of data

the damages but also quantify the damages when the full set of modes is available.

To demonstrate the advantages of the proposed method over the classical deflection flexibility difference method, the percentage changes in the diagonal elements of the difference in classical deflection flexibility before and after damages are plotted against nodes in Fig. 5(b). It is difficult to identify the damage member from this figure. This is because change in classical flexibility is manifested as DOF characterization, and each DOF is connected with many members for this truss.

4.1.2.2. Results from simulated data

The simulated data was utilized to validate the performance of the AS flexibility difference method. Herein, modal parameters were obtained by modal parameter identification from simulated acceleration and excitation data. Structural damping was assumed to be Rayleigh damping with damping ratio of 1% for each mode. The truss was excited by limited-band random white noise (0-1000Hz) applied at all nodes. The Newmark-Beta integration was used to compute the acceleration responses at all nodes. The acceleration and excitation data was sampled at a rate of 1152 Hz, and 60 seconds signals were obtained. To simulate the practical field conditions, Gaussian white noise with the mean value of zero and the

Root-Mean-Square (RMS) equal to 5% of that of the responses was added to the acceleration responses.

The procedures to detect damage using the AS flexibility difference method are as follows. First, Eigensystem Realization Algorithm (ERA) is employed to identify the modal frequencies and translational mode shapes. And then mode shapes are normalized with respect to mass matrix, or each mode shape is normalized by the length of the corresponding mode shape. Second, the axial strain mode shapes are computed from the normalized mode shapes by Eq. (9) and the AS flexibilities for the intact and

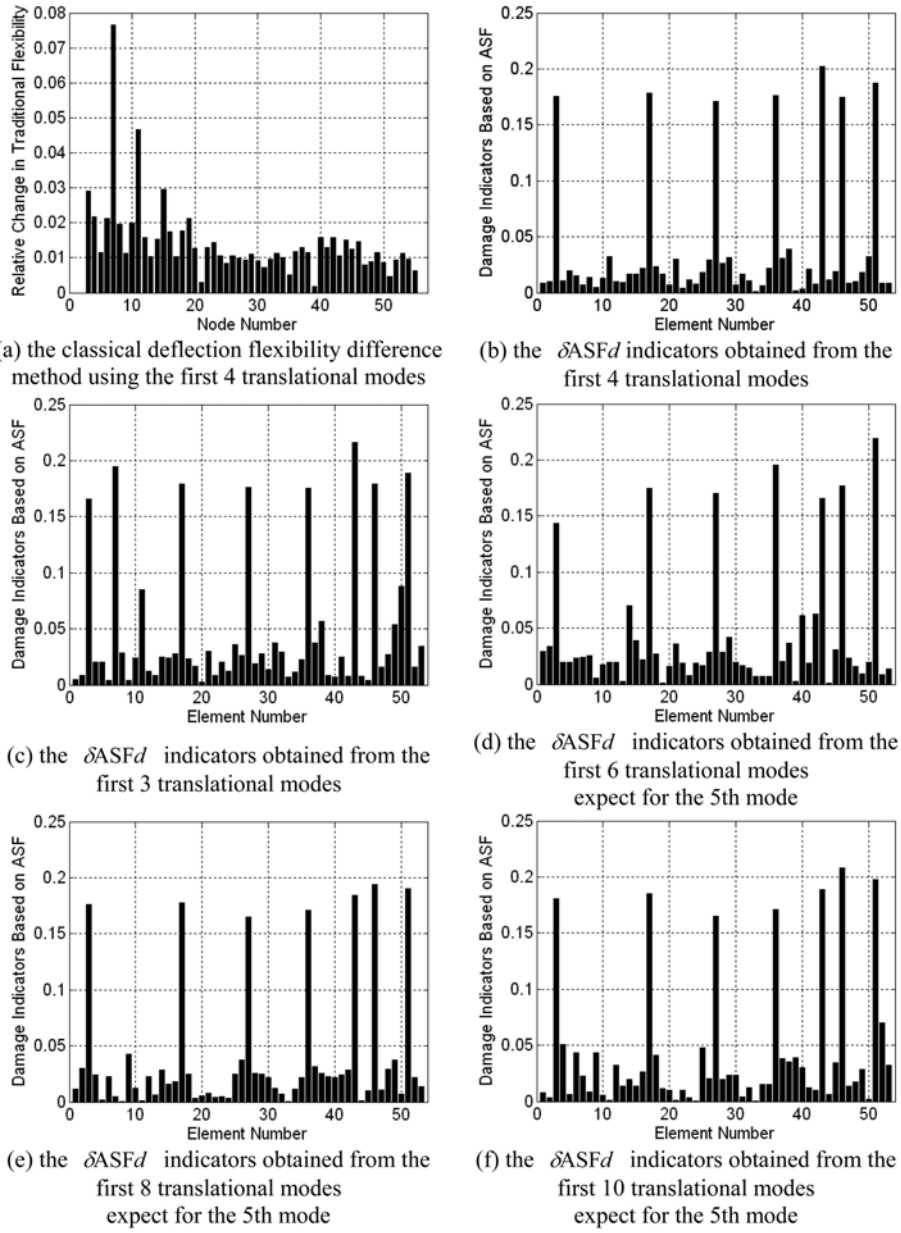

(a) the classical deflection flexibility difference method using the first 4 translational modes

(b) the δASFd indicators obtained from the first 4 translational modes

(c) the δASFd indicators obtained from the first 3 translational modes

(d) the δASFd indicators obtained from the first 6 translational modes expect for the 5th mode

(e) the δASFd indicators obtained from the first 8 translational modes expect for the 5th mode

(f) the δASFd indicators obtained from the first 10 translational modes expect for the 5th mode

Fig. 6 Damage detection results by the AS flexibility difference method using different numbers of translational modes

damaged trusses are assembled by Eq. (10). Finally, the damage indicators δASFd are extracted by Eq. (15) and the members that have large magnitudes in the δASFd indicators are associated with the potential damage members within the structure.

For the intact and damage cases, the lower 10 natural frequencies, damping ratios and EMAC indices identified from the simulated data by ERA were summarized in Table 1. The identification accuracy was evident from a cursory examination of damping ratio and EMAC index of each mode. From the table, the natural frequencies of the damaged truss differ from those of the intact truss by less than 1.17%.

The damage detection by the AS flexibility difference method was performed using different numbers of modes, respectively. Some typical results are presented in Figs. from 6(b) to 6(f). From these figures, we conclude that: (1) If the modes used are less than or are equal to three, apart from the δASFd indicators of the damaged elements, the δASFd indicators associated with some undamaged elements are also much larger than other δASFd indicators nearby. For example, if the first three modes are used, the 7th and 11th elements are mistakenly identified as damaged elements from Fig. 6(c). (2) If the number of the modes used are larger than three, only the δASFd indicators associated with the damaged elements are much larger than others. For example, the δASFd indicators obtained from the first four modes provide good information on the damage sites, as shown in Fig. 6(b). (3) When higher frequency modes are used, one can find from Figs. from 6(d) to 6(f) that the more the modes are used, the better the results are obtained. In addition, from Figs. 6(b), 6(d), 6(e) and 6(f), we approximately estimate that the damage extents in each damaged element are approximately equal.

For comparison purpose, the damage detection results using the classical deflection flexibility difference are shown in Fig. 6(a). It is evident that one can't locate the potential damage sites from this figure.

In general, the results shown in Fig. 6 tell us that: the proposed AS flexibility is more viable for damage detection than classical deflection flexibility.

4.1.2.3. The effects of the number of measurement sensors

To investigate the robustness of the method in the face of sparse data, acceleration responses of different numbers of measurement points were used to simulate that the measurement DOFs were not complete. Various cases with different measurement points were considered in this study shown in Fig. 7 and the first four identified modes were used for each case.

The δASFd indicators for these cases are plotted against elements in Figs. 7(a)-(d), respectively. From Fig. 7(a), it is found the δASFd indicator associated with the 3rd element is much larger than those associated with the other 8 elements. It suggests that the 3rd element is potentially damaged. Assuming that only the responses in the x direction at the nodes of each upper chord member are measured, the 17th element is identified as a potentially damaged element, as shown in Fig. 7(b). Similarly, among the lower chord members, the 27th and 36th elements are potentially damaged, as shown in Fig. 7(c). When only the responses in both the x and y directions at the nodes in the first five bays are measured, it is found that the 3rd, 17th, 27th and 43rd elements are potentially damaged, shown in Fig. 7(d). Consequently, for a given group of members, only if the axial responses of the two nodes of each member are measured, the extracted δASFd indicator tells whether it is damaged.

In practical applications, we can make the best use of the limited number of measurement sensors by the following ways: (1) to deploy all the sensors available on the nodes in a region of the structure to make the measurement DOFs in this region be complete, and then move these sensors to other regions of the structure, sequentially. In this case, damaged members in each region can be identified sequentially. (2) or to place all the sensors on the nodes of the members interested. For example, if one

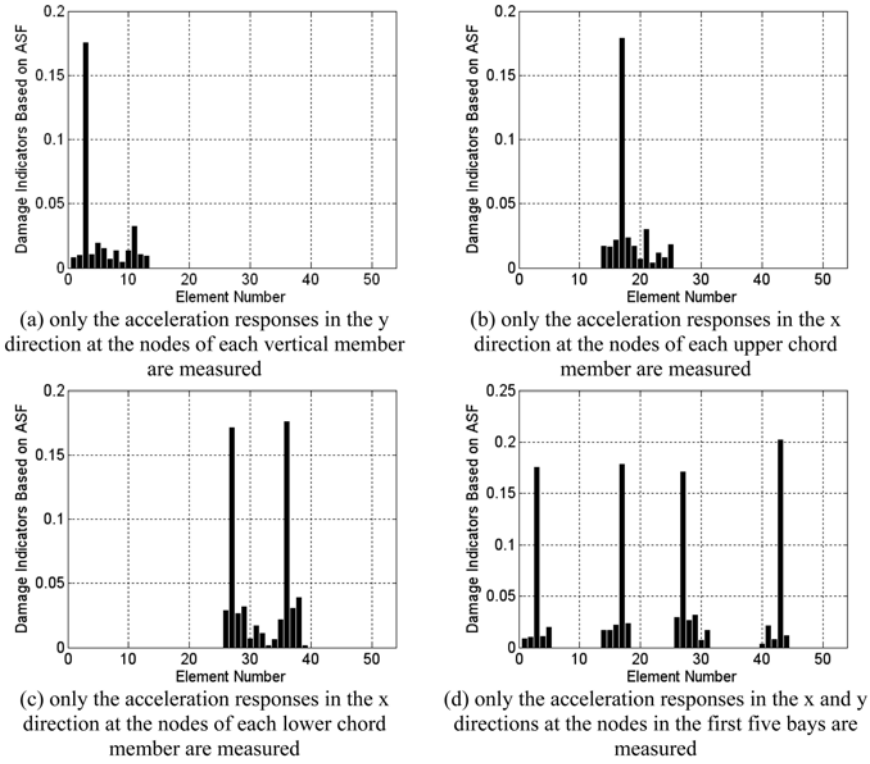

Fig. 7 The damage detection results by the AS flexibility difference method when measurement DOFs and measurement modes are not complete

just wants to know the health conditions of the upper chord members of this truss, only to deploy the sensors on the nodes of the upper chord members to measure the responses in the horizontal direction.

4.1.3. The damage detection results by the DLV approach based on the AS flexibility

The procedures for damage detection using the DLV approach based on the AS flexibility are as follows. First, to obtain the DLVs through the SVD of the change in AS flexibilities from the damaged to undamaged states; Second, to apply the DLVs in the form of a pair of axial forces with equal amplitudes but opposite directions on each member of the undamaged truss, and then to calculate the generalized internal force in each member. The elements whose generalized internal forces are close to zero can be identified as damaged ones.

4.1.3.1. Results from analytical data

The analytical data was used to compare the performances of the three GIFs defined in this paper. When the full set of modes are used, the generalized internal forces (GIFs) obtained by Eq. (17), Eq. (18) or Eq. (19) are plotted against elements in Figs. from 8(b) to 8(d), respectively. From Figs. 8(c) and 8(d), one can localize the seven damage sites using the GIF defined by Eq. (18) and Eq. (19). Furthermore, the damage location results using the GIF defined by Eq. (19) are a little better than those from the GIF defined by Eq. (18). However, the GIF defined by Eq. (17) seems not to be reasonable, as shown in Fig. 8(b). For brevity, only the GIF defined by the Eq. (19) will be presented in the following results.

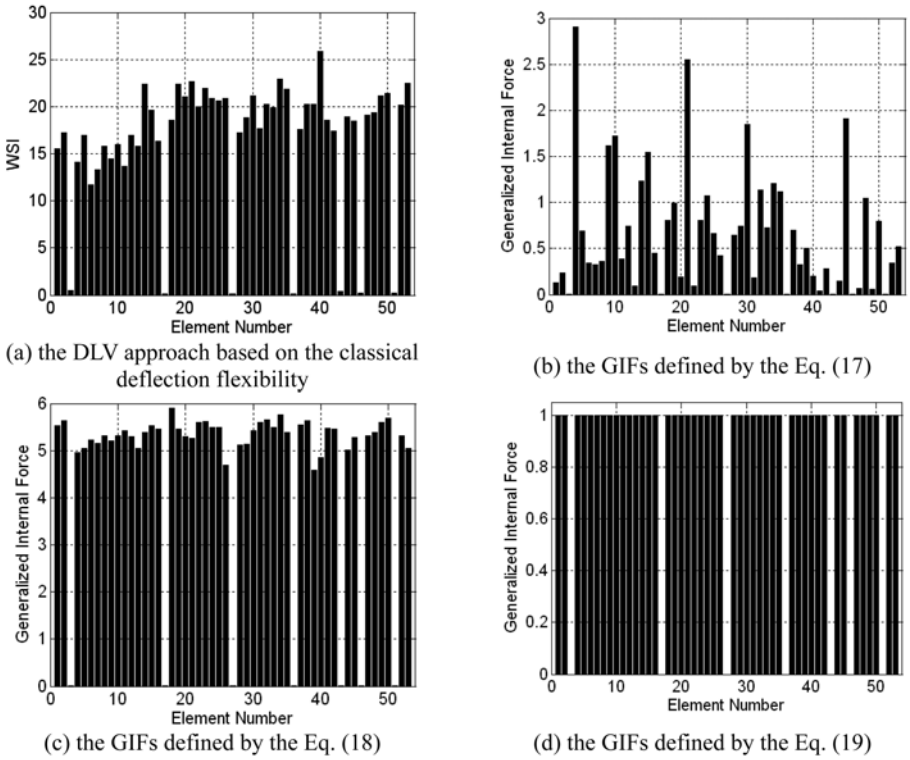

(a) the DLV approach based on the classical deflection flexibility

(b) the GIFs defined by the Eq. (17)

(c) the GIFs defined by the Eq. (18)

(d) the GIFs defined by the Eq. (19)

Fig. 8 Damage localization results by the DLV approaches using all the 53 translational modes

From Fig. 8(d), we also find that when the full set of modes are used to assemble the AS flexibility, the GIFs obtained by the Eq. (19) associated with undamaged elements are equal to 1 and the GIFs of the damaged elements are 0. This is because $\mathbf{V}_0$ is orthogonal.

The damage location results using the DLV approach based on the classical deflection flexibility are also presented, as shown in Fig. 8(a). "WSI" is the index showing the stress induced by DLVs. Large WSI indicates large stress in the element, and vice versa. The elements with small WSIs are potentially damaged elements. It is obvious that the DLV method based on the classical deflection flexibility also finds all the seven damage sites when the complete set of modes is used.

4.1.3.2. Results from simulated data

The simulated data was used to compare the performance of the DLV approach based on the AS flexibility with that of the DLV approach based on classical deflection flexibility. The numerical simulation process of modal test was the same as Section 4.1.2.

Fig. 9 presents the damage location results by the two DLV approaches when different numbers of modes are used. When the first 4 modes are available, although only four damage sites (the 17th, 27th, 36th and 43rd elements) are identified by both approaches, the extent that the GIFs of the damaged elements are lower than those of the undamaged elements, shown in Fig. 9(a), is much larger than the extent that the WSIs of the damaged elements are lower than those of the undamaged elements, in Fig. 9(b). From Fig. 9(c), though the GIF in the 3rd element is not close to zero, it is much smaller than other GIFs nearby and thus the 3rd element is identified as a potentially damaged element. Thus, the former

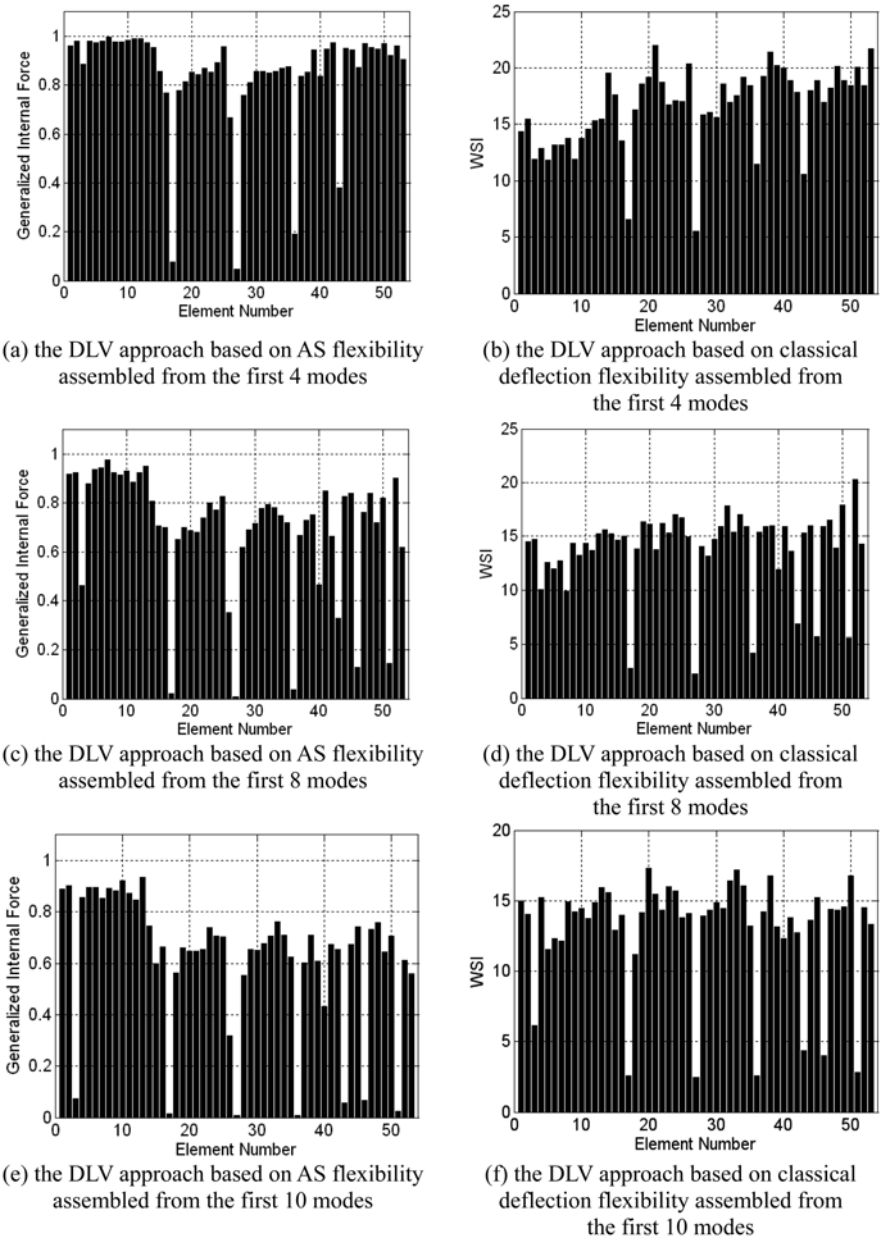

(a) the DLV approach based on AS flexibility assembled from the first 4 modes

(b) the DLV approach based on classical deflection flexibility assembled from the first 4 modes

(c) the DLV approach based on AS flexibility assembled from the first 8 modes

(d) the DLV approach based on classical deflection flexibility assembled from the first 8 modes

(e) the DLV approach based on AS flexibility assembled from the first 10 modes

(f) the DLV approach based on classical deflection flexibility assembled from the first 10 modes

Fig. 9 Damage localization results using the DLV approaches when different numbers of modes are used

has successfully localized all seven damage sites when the first eight modes are used, while the latter just identify six damage sites with the same number of modes shown in Fig. 9(d). Both approaches locate all seven damages when the first 10 modes are available, but the GIFs in the damaged elements are much closer to zero than the WSIs of the corresponding elements, as shown in Figs. 9(e) and 9(f). Therefore, the DLV approach based on AS flexibility performs much better than that based on classical deflection flexibility.

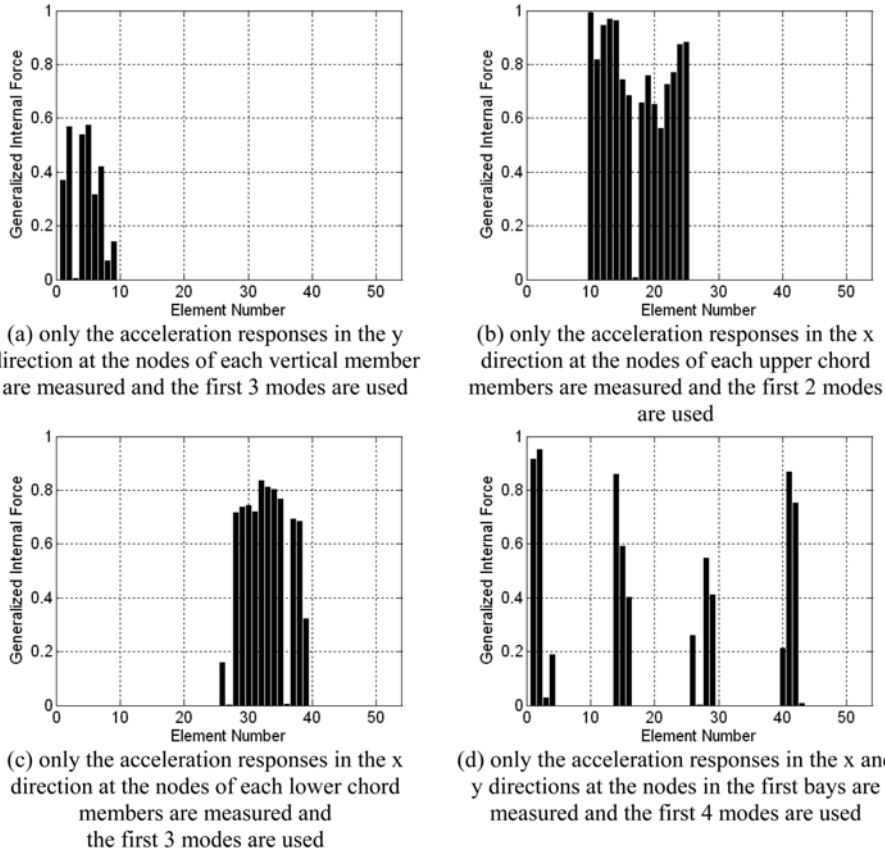

(a) only the acceleration responses in the y direction at the nodes of each vertical member are measured and the first 3 modes are used

(b) only the acceleration responses in the x direction at the nodes of each upper chord members are measured and the first 2 modes are used

(c) only the acceleration responses in the x direction at the nodes of each lower chord members are measured and the first 3 modes are used

(d) only the acceleration responses in the x and y directions at the nodes in the first bays are measured and the first 4 modes are used

Fig. 10 The damage localization results by the DLV approach based on the AS flexibility when measurement DOFs and measurement modes are not complete

4.1.3.3. The effects of the number of measurement sensors

To investigate the effects of the number of measurement points on the DLV approach based on AS flexibility, the cases with different numbers of measurement points used in Section 4.1.2 were considered here.

The Generalized Internal Forces (GIFs) in the measured members for these cases are plotted in Figs. 10(a)-(d). In each figure, the GIFs in the damaged elements are close to zero when few modes are used. It is obvious that this method has successfully identified the potentially damaged elements occurred in the measured regions for each case. Consequently, for a given group of members, only if the axial responses of the two nodes of each member are measured, the damaged members among the measured ones are identified from the GIFs with small magnitudes. Compared with the DLV approach based on classical deflection flexibility, the way of sensor placement is more flexible.

4.2. Example #2: A 5-story steel-frame structure

To further demonstrate the performance of the proposed AS flexibility in detecting damages occurred in frame structures, the analytical model of a 5-story, 1-bay by 2-bay steel-frame structure, as shown in Fig. 11(a), was studied.

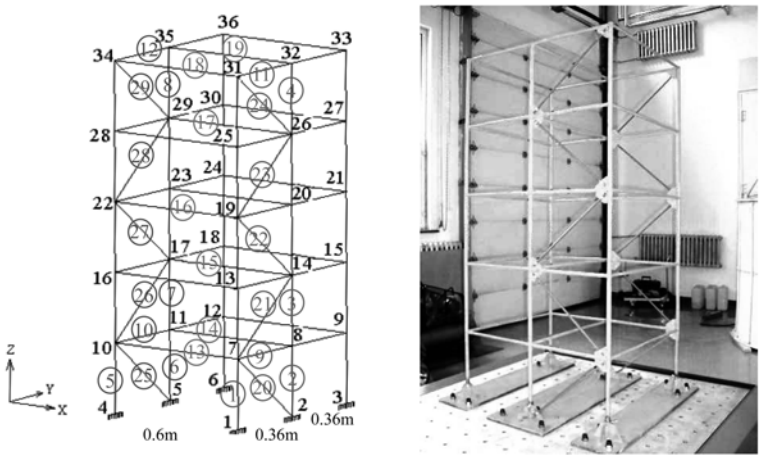

(a) Diagram of analytical model (b) Prototype building structure

Fig. 11 A 5-story steel-frame structure

Table 2 Properties of structural members

Property	Columns	Beams	Braces
Cross-sectional area (m^2)	8.796×10^{-5}	6.283×10^{-5}	2.199×10^{-5}
Moment of inertia I_y (m^4)	2.199×10^{-9}	8.168×10^{-10}	0
Moment of inertia I_z (m^4)	2.199×10^{-9}	8.168×10^{-10}	0
Young's Modulus (Pa)	2.0×10^{11}	2.0×10^{11}	2.0×10^{11}
Mass density (kg/m^3)	7.85×10^{3}	7.85×10^{3}	7.85×10^{3}
Possion ratio	0.3	0.3	0.3

Table 3 Typical damage cases in the numerical simulation

	Damage patterns
Case 1	Brace 2-7 in the first story (Member No. 20) is removed.
Case 2	Brace 7-14 in the second story (Member No. 21) is removed.
Case 3	Brace 2-7 in the first story (Member No. 20), brace 7-14 in the second story (Member No. 21) and brace 19-26 in the fourth story (Member No. 23) are removed.
Case 4	Braces 2-7 and 5-10 in the first story (Member No. 20 and 25) are removed.
Case 5	Vertical member 2-8, vertical member 5-11, brace 2-7 and brace 5-10 in the first story (Member No. 2, 6, 20 and 25) are removed.
Case 6	Vertical members 8-14 and 11-17 in the second story (Member No. 3 and 7) are removed.

4.2.1. The analytical model

The prototype building structure of the steel-frame structure, shown in Fig. 11(b), is in the laboratory of School of Civil Engineering at Harbin Institute of Technology. It had a 0.6 m×0.72 m plan and was 1.5 m tall. It had fixed supports. The members were made of Grade Q345 steel. The sections were tube-shape with properties as listed in Table 2.

The finite element model (FEM) based on this structure was developed to generate the simulated data. The node numbering involved in the FEM was illustrated in Fig. 11(a). Columns and beams were

Table 4 The analytical natural frequencies for the intact and all damaged cases (Hz)

	Intact	Case 1	Case 2	Case 3	Case4	Case5	Case 6
1	10.79	10.791	10.796	10.838	10.791	10.086	10.086
2	28.818	25.736	24.861	18.706	24.39	17.196	17.196
3	37.387	37.409	37.507	35.271	34.507	18.522	18.522
4	51.482	41.2	40.059	37.589	37.431	34.446	34.446
5	64.372	51.55	51.531	51.134	46.638	40.809	40.809
6	70.327	64.379	64.474	64.801	51.668	50.462	50.462
7	75.758	73.358	73.383	71.816	64.389	62.494	62.494
8	76.009	76.066	76.342	73.784	76.138	62.581	62.581
9	79.864	79.974	80.096	76.706	80.088	65.826	65.826
10	88.961	89.231	89.233	80.217	89.509	69.547	69.547

modeled as Euler-Bernoulli beams and diagonal braces were modeled as bars (no bending stiffness). Because it was difficult to measure structural rotational responses in practice, these rotational DOFs at each node were reduced from the FEM and then there were 3 translational DOFs at each node in the reduced FEM. Assume that the structure had Rayleigh damping and the damping ratio of each mode was 1%.

In this example, damages were simulated by removing the braces or the following vertical members: vertical members 2-8, 8-14, 5-11 and 11-17. Six typical damage patterns with different numbers of members removed were specified, as listed in Table 3. The analytical natural frequencies for the undamaged and damaged cases are listed in Table 4.

Numerical simulation of modal test was similar to Section 4.1.2. Limited-band (0-400Hz) white noise was used to excite the structure to simulate that the structure was subjected to ambient excitation at each floor in the y direction. Assume that three-direction accelerometers were placed at the following 14 nodes: Nodes 7, 8, 10, 11, 14, 17, 19, 22, 26, 29, 31, 32, 34 and 35. The detectable members were indicated by the number in a circle, as shown in Fig. 11(a). The Newmark-Beta time history analysis was employed to compute the acceleration responses at measurement sensor locations. It was assumed that the acceleration responses were recorded at a sampling rate of 512 Hz and the sampling time was 20 seconds. To simulate measurement noises, Gaussian white noise with the mean value of zero and the RMS equal to 5% of that of the responses was added to the acceleration responses.

Table 5 The modal parameters identified from simulated data by ERA

	Order	Frequency (Hz)	Damping ratio (%)	EMAC
Case 1	1	25.7313	1.0241	74.4209
	2	41.1952	1.0222	70.8027
Case 2	1	24.8552	1.0510	90.1269
	2	40.0513	1.0148	40.6460
Case 3	1	18.7075	1.1597	61.3791
	2	35.2685	1.0584	68.4654
Case 4	1	34.4997	1.0448	82.5943
Case 5	1	18.5203	1.0997	72.9883
Case 6	1	22.3560	1.0492	73.6821

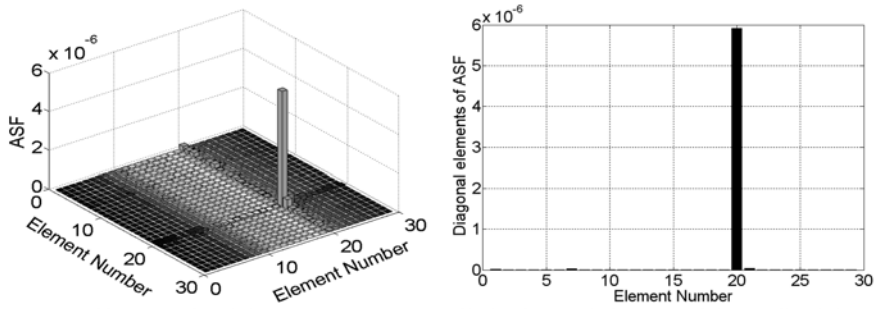

(a) the AS flexibility matrix (b) the diagonal elements of the AS flexibility

Fig. 12 Brace 2-7 in the first story (Member No. 20) is removed

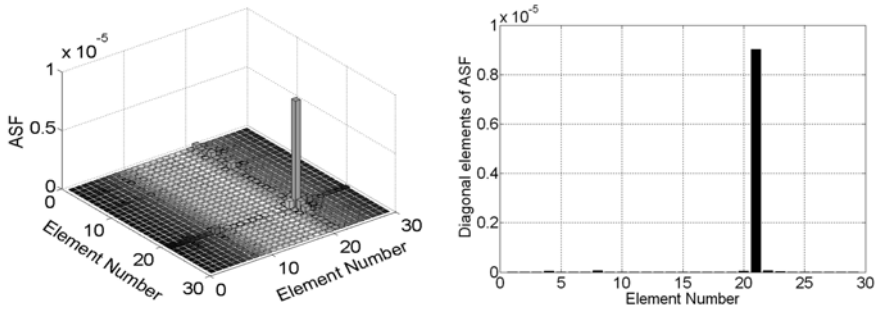

(a) the AS flexibility matrix (b) the diagonal elements of the AS flexibility

Fig. 13 Brace 7-14 in the second story (Member No. 21) is removed

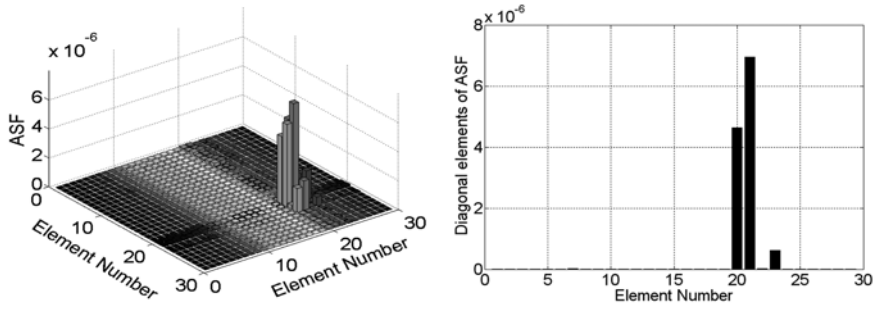

(a) the AS flexibility matrix (b) the diagonal elements of the AS flexibility

Fig. 14 Brace 2-7 in the first story, brace 7-14 in the second story and brace 19-26 in the fourth story (Member No. 20, 21 and 23) are removed

The modal parameter identification was carried out by ERA. The identified modal parameters for the damaged cases are listed in Table 5. For the undamaged case, no modes were identified from the current simulated data. For Cases from 1 to 3, two modes were identified from the simulated data, and for Cases from 4 to 6, one mode was identified.

4.2.2. The damage detection results by the damaged AS flexibility

Because the baseline data was not obtained from the simulated data, damage sites were directly identified by the maximum values of the diagonal elements of the damaged AS flexibility. For each

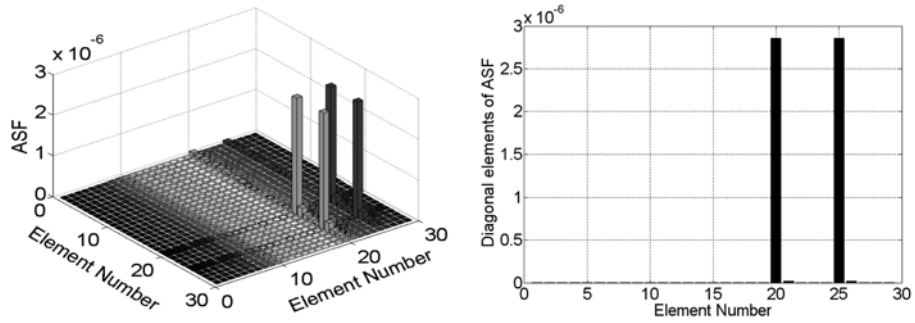

(a) the AS flexibility matrix (d) the diagonal elements of the AS flexibility

Fig. 15 Braces 2-7 and 5-10 in the first story (Member No. 20 and 25) are removed

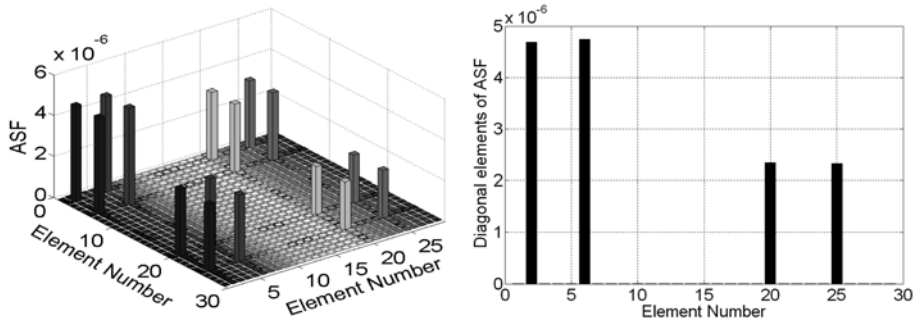

(a) the AS flexibility matrix (b) the diagonal elements of the AS flexibility

Fig. 16 Vertical member 2-8, vertical member 5-11, brace 2-7 and brace 5-10 in the first story (Member No. 2, 6, 20 and 25) are removed

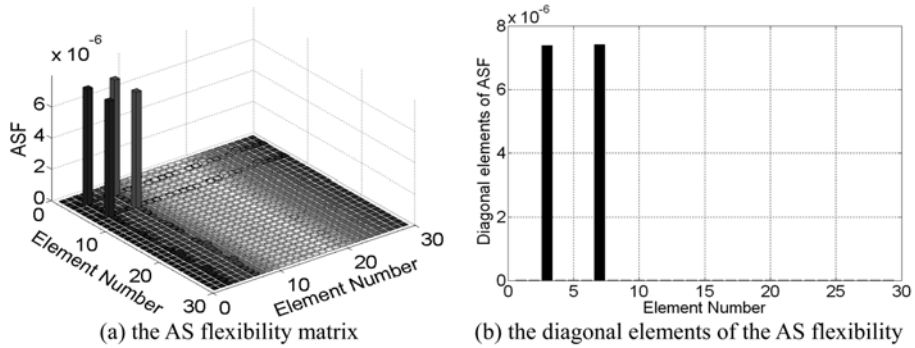

(a) the AS flexibility matrix (b) the diagonal elements of the AS flexibility

Fig. 17 Vertical members 8-14 and 11-17 in the second story (Member No. 3 and 7) are removed

damage case, the AS flexibility was assembled from the identified modes, and the AS flexibility matrix and their diagonal elements are plotted in Figs. from 12 to 17. In each figure, the diagonal elements associated with the damaged member are much larger than others. It is obvious that the potentially damaged member is directly identified by the damaged AS flexibility when only one or two lower frequency modes are available. From Figs. 15, 16 and 17, it can be observed that if two symmetrical members are removed, the magnitudes of the diagonal elements corresponding to the two members are equal.

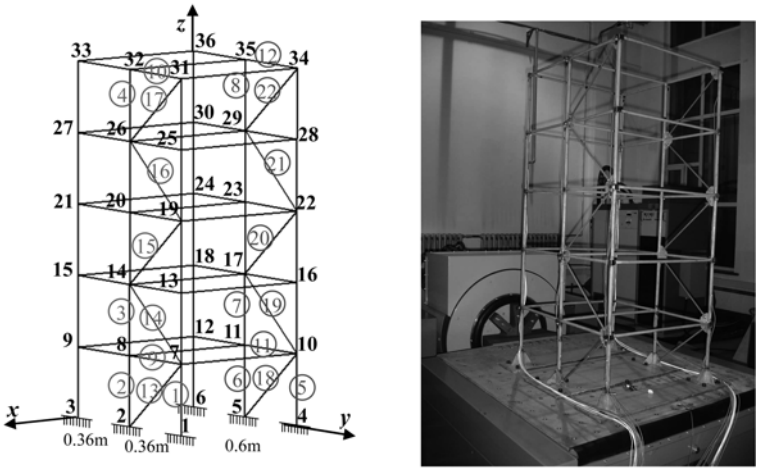

(a) Diagram of analytical model (b) Sensor locations

Fig. 18 A five-story steel-frame structure in the experiment

5. Experimental application

To demonstrate the effectiveness of the proposed AS flexibility on damage localization, experiments were conducted on the 5-story, 1-bay by 2-bay steel-frame structure described in Section 4.2. The structural parameters of the steel-frame structure refer to Section 4.2 and its finite element model is shown as Fig. 18(a).

5.1. Description of experiment

The experiment setup mainly consisted of shaking table (produced by UD company, USA) and some three-direction accelerometers (produced by PCB Companay, USA). These three-direction accelerometers were mounted on the structure using glue at the following 14 nodes: Nodes 7, 8, 10, 11, 14, 17, 19, 22, 26, 29, 31, 32, 34 and 35, as shown in Fig. 18. Because the x-direction channels of some sensors failed to record responses, only the 22 members indicated by the number in a circle could be detected, shown in Fig. 18(b).

Table 6 Simulated cases in the experiment

	Damage patterns
Case 1	Vertical members 2-8, vertical member 5-11, brace 2-7 and brace 5-10 in the first story (Member No. 2, 6, 13 and 18) are removed.
Case 2	Braces 2-7 and 5-10 (Member No. 13 and 18) in the first story are removed.
Case 3	Brace 2-7 in the first story (Member No. 13) is removed.
Case 4	Brace 7-14 in the second story (Member No. 14) is removed.
Case 5	Brace 2-7 in the first story, brace 7-14 in the second story and brace 19-26 in the fourth story (Member No. 13, 14 and 16) are removed.
Case 6	Undamaged

Table 7 The modal parameters identified from experimental data by ERA

	Order	Frequency (Hz)	Damping ratio (%)	EMAC(%)
Case 1	1	18.78	2.7972	96.262
Case 2	1	34	3.3944	95.876
Case 3	1	43.09	2.324	75.449
Case 4	1	40.645	1.1269	96.343
Case 5	1	35.329	1.0114	96.878

Damages in the frame were introduced by removing some braces or some vertical members. Five typical damage patterns with different numbers of members removed are specified in Table 6.

For each case, the structure was subjected to Band-limited (0-1000Hz) white noise, and structural acceleration responses and shaking table responses were recorded. The sampling frequency of acceleration responses was 2560 Hz and the sampling duration was 120 seconds.

5.2. Experimental results

For each case, taking the responses acquired from the sensor on the shaking table as input and the responses acquired from each sensor mounted on the structure as output, the structural frequency response function was obtained. And then Eigensystem Realization Algorithm was employed to identify the

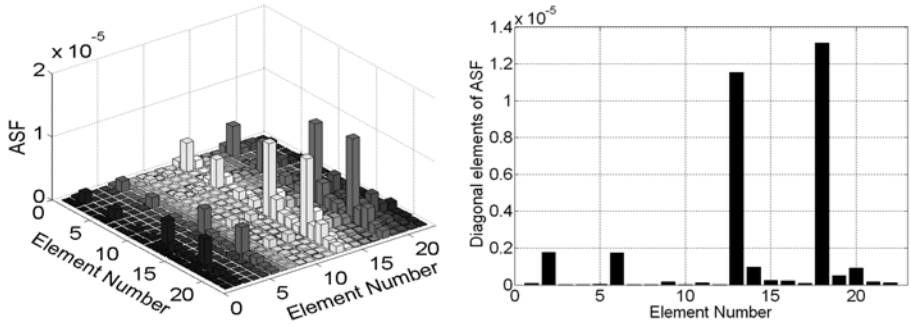

(a) the AS flexibility matrix (b) the diagonal elements of the AS flexibility

Fig. 19 Vertical members 2-8 and 5-11, braces 2-7 and 5-10 in the first story (Member No. 2, 6, 13 and 18) are removed in the experiment

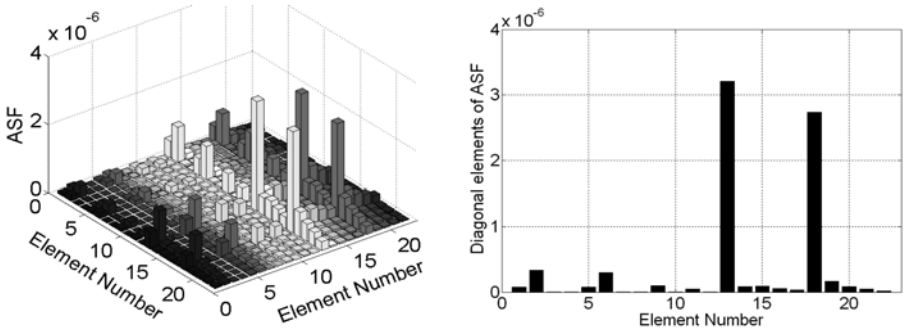

(a) the AS flexibility matrix (b) the diagonal elements of the AS flexibility

Fig. 20 Braces 2-7 and 5-10 in the first story (Member No. 13 and 18) are removed in the experiment

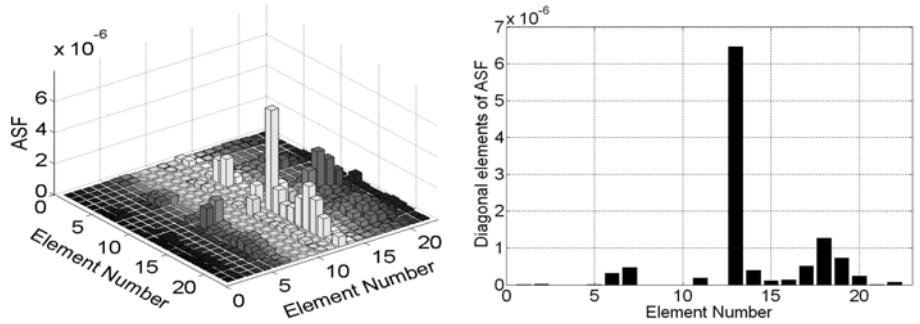

(a) the AS flexibility matrix (b) the diagonal elements of the AS flexibility

Fig. 21 Brace 2-7 in the first story (Member No. 13) is removed in the experiment

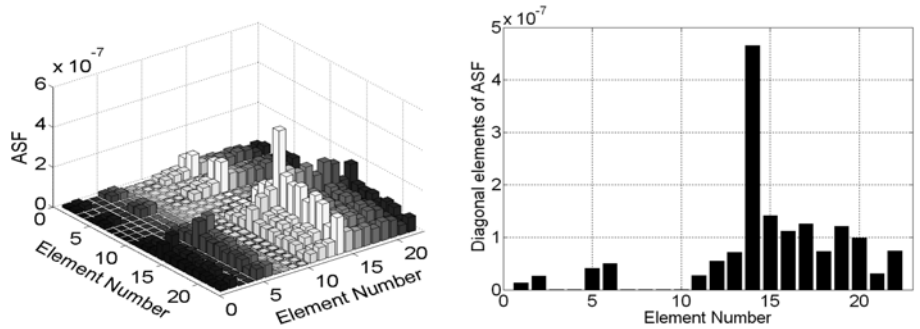

(a) the AS flexibility matrix (b) the diagonal elements of the AS flexibility

Fig. 22 Brace 7-14 in the second story (Member No. 14) is removed in the experiment

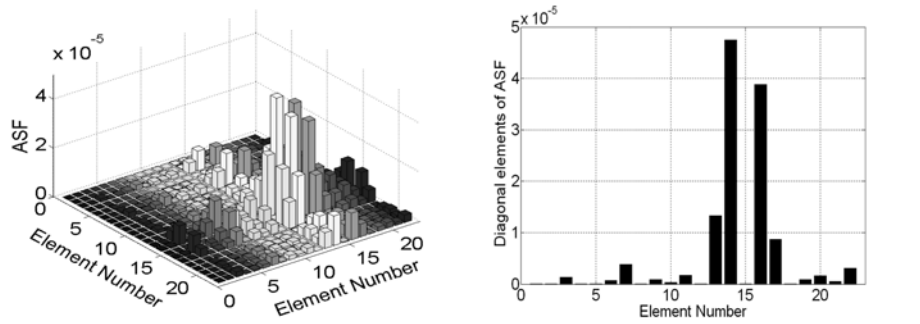

(a) the AS flexibility matrix (b) the diagonal elements of the AS flexibility

Fig. 23 Brace 2-7 in the first story, brace 7-14 in the second story and brace 19-26 in the fourth story (Member No. 13, 14 and 16) are removed in the experiment

modal parameters. Table 7 presents the identified natural frequencies and damping ratios of the first mode in the y direction for each case. Next, the AS flexibilities for each damage case were assembled from the identified modes.

Because the baseline modal parameters were not obtained from the experiment data, damage sites were identified by the maximum values of the diagonal elements of the damaged AS flexibility. The AS flexibility matrices and their diagonal elements for all simulated cases in the experiment are plotted in Figs. from 19 to 23, respectively. For Cases from 1 to 4, the diagonal elements corresponding with the

damaged members are much larger than those corresponding with the undamaged members, as shown in Figs. from 19 to 22. It suggests that the potential damage members are directly identified from the maxima of the diagonal elements of the damaged AS flexibility.

However, the results obtained from the experiment data were not as good as those obtained from analytical data in Section 4.2.2. For example, it was found that the diagonal elements associated with some undamaged members were not close to zero. Some reasons were responsible for it. First, measurement noises existed during the experiment; second, there were some differences between the analytical model and the real structure.

For Case 5, the diagonal elements corresponding to the 13th, 14th, 16th and 17th members are much larger than others, as shown in Fig. 23, and it suggests the four members are damaged. In fact, only the 13th, 14th and 16th members were removed in this case. This might be due to the fact that the excitation density was lower in this case during the test and the signal-to-noise ratio was lower.

6. Conclusions

For damage detection of structures whose internal forces are dominated by axial forces, the Axial Strain (AS) flexibility is proposed and formulation to synthesize AS flexibility by identified translational modes is derived. The AS flexibility matrix is diagonal for statically determined structures, and is dominated by diagonal elements for statically underdetermined structures. Three damage detection techniques, i.e., the AS flexibility difference method, the DLV method based on AS flexibility and the direct method using the damaged AS flexibility, are developed. Conclusions from this study are summarized as follows:

1) Since each element in AS flexibility is associated with a structural member or element instead of a structural DOF, these methods can localize damages to exact elements for truss or frame structures;
2) The proposed AS flexibility is better than classical deflection flexibility for damage detection. Furthermore, the AS flexibility difference method performs better than the DLV method based on the AS flexibility by the example of 14-bay planar. Both methods locate the damages and the former also identifies the relative damage severity;
3) In practical applications, for both truss and frame structures, if baseline data are not readily obtained, the potential damage sites are directly identified from the maximum values of the diagonal elements of the damaged AS flexibility;
4) These proposed methods only require few lower frequency modes;
5) Only if both the axial responses at the two nodes of a given element are measured, the proposed methods can tell whether the element is damaged. That is to say, the method is well suited to sparse data;

However, the capability of the proposed method depends on the quality of the measured data and the accuracy of the identified modal parameters.

Acknowledgements

The authors would like to acknowledge the National Natural Science Foun dation of China for financial support under Grant no. (50579008 and 50708029) and the 41st Post-doc. Science Foundation of China.

References

Bernal, D. and Gunes, B. (2002), "Damage localization in output-only systems: a flexibility based approach", *Proc. of IMAC-XX*.

Bernal, D. and Gunes, B. (2004), "Flexibility based approach for damage characterization: benchmark application", *J. Eng. Mech.*, **130**(1), 61-70.

Doebling, S.W. and Farrar, C.R. (1996), "Computation of structural flexibility for bridge health monitoring using ambient modal data", *Proc. of 11th ASCE Engineering Mechanics Conf*.

Doebling, S.W. and Peterson, L.D. (1997), "Computing statically complete flexibility from dynamically measured flexibility", *J. Sound Vib.*, **205**(5), 631-645.

Doebling, S.W., Peterson, L.D. and Alvin, K.F. (1996), "Estimation of reciprocal residual flexibility from experimental modal data", *AIAA J.*, **34**(8), 1678-1685.

Doebling, S.W., Peterson, L.D., Alvin, K.F. (1998), "Experimental determination of local structural stiffness by disassembly of measured flexibility matrices", *J. Vib. Acoust.*, **120**, 949-957.

Duan, Z.D., Yan, G.R. and Ou, J.P. (2005), "Structural damage detection using the angle-between-string-and-horizon flexibility", *Proc. of the 2nd Int. Conf. on Structural Health Monitoring and Intelligent Infrastructure*, Shenzhen, China, November.

Duan, Z.D., Yan, G.R., Ou, J.P. and Spencer, B.F. (2005), "Damage localization in ambient vibration by constructing proportional flexibility matrix", *J. Sound Vib.*, **284**(1-2), 455-466.

Gao, Y. and Spencer, B.F. (2002), "Damage localization under ambient vibration using changes in flexibility", *J. Earthq. Eng.*, **1**(1), 136-144.

Long, Y. and Bao, S. (1996), *Structural mechanics*, Higher education publishing company.

Pandey, A.K., Biswas, M. (1994), "Damage detection in structures using changes in flexibility", *J. Sound Vib.*, **169**(1), 3-17.

Pandey, A.K., Biswas, M. (1995), "Experimental verification of flexibility difference method for locating damage in structures", *J. Sound Vib.*, **184**(2), 311-328.

Park, K.C. and Felippa, C.A. (1998), "A variational framework for solution method developments in structural mechanics", *J. Appl. Mech.,* **65**(1), 242-249.

Park, K.C., Reich, G.W. and Alvin, K.F. (1997), *Damage detection using localized flexibilities, structural health monitoring, current status and perspectives*, F.K. Chang, Technomic Publishers.

Reich, G.W. and Park, K.C. (2000), "Experimental application of a structural health monitoring methodology", *Proc. of SPIE*, In Smart Structures and Materials.

Sim, S.H. and Spencer, Jr. B.F. (2007), "Multi-scale sensing for structural health monitoring", *World Forum on Smart Materials and Smart Structures Technology*.

BS